

---

# A COST-EFFECTIVE STRATEGY FOR IN-FLIGHT TRAJECTORY PREDICTIONS OF MULTI-BODY CONFIGURATIONS

Shlomy Shitrit<sup>1</sup> and Yossef Elimelech<sup>2</sup>

*RAFAEL, Advanced Defense Systems, Ltd., Haifa 31021, Israel*

*Soreq NRC, Yavne 81800, Israel*

In the present work we study the dynamics of a supersonic missile canopy, separated in-flight. We distinguish between three separation phases: rotation about a fixed hinge, canopy-missile reciprocity, and free-canopy flight regime. The complementary numerical investigation conducted is two-fold. First, a segregated scheme is considered where an aerodynamic model, embodying the different flight phases, is constructed and introduced into a tailored three degrees-of-freedom (3DOF) rigid-body simulation. The aerodynamic model, obtained by quasi-steady RANS computations, consists of various canopy positions and orientations at specified flight conditions, to facilitate high fidelity trajectories based on a lean and efficient dataset. Then, a coupled unsteady-flow and multi-body dynamics framework is considered, and the realized canopy trajectories are compared with those obtained by the segregated approach to a satisfying agreement. The suggested scheme is shown to be beneficial to the robust design of canopy separated configurations.

**Keywords:** Trajectory predictions, Multi-body aerodynamic, CFD applications, Shroud separation, Supersonic missile aerodynamic

## Nomenclature

$M$	=	Mach number
$\alpha$	=	angle of attack, deg
$\beta$	=	side-slip angle, deg
$\theta$	=	opening angle, deg
$\rho$	=	density, kg/m <sup>3</sup>
$u, v, w$	=	velocity components, m/s
$\omega$	=	angular velocity, rad/s
$m$	=	mass, kg
$h$	=	angular momentum,
$p$	=	static pressure, Pa ; order of convergence
$E$	=	energy, J
$R$	=	residual
$Rey$	=	Reynolds number
$DOF$	=	degrees of freedom
$y+$	=	yplus
$Cl$	=	lift coefficient
$Cd$	=	drag coefficient
$Cm$	=	pitch moment coefficient
$Cn$	=	normal force coefficient
$Cy$	=	side force coefficient

---

<sup>1</sup> Research Engineer, CFD group, Aeronautical Systems, P.O. Box 2250, Israel; shlomy.shitrit@gmail.com

<sup>2</sup> Yossef Elimelech, Soreq NRC, Yavne 81800, Israel; yossefel@soreq.gov.il

$C_x$	=	axial force coefficient
$D$	=	missile's body diameter, m
$GCI$	=	grid convergence index
$N$	=	mesh size
$S$	=	area, m <sup>2</sup>
$L$	=	grid level

*Subscripts*

<i>baseline</i>	=	initial configuration
<i>ref</i>	=	reference value

## I. INTRODUCTION

The increased missiles performance parameters (compared to airplanes) may introduce aerodynamic problems which are aerodynamic heating, higher dynamic pressures, higher maneuvering accelerations, etc. Since different missions are involved, missiles are designed to compensate these arising aerodynamic related problems. Especially air-to-air missiles are designed to operate at high Mach numbers, and at these extreme flow regimes the missile's nose is exposed to significant aerodynamic heating which can damage the electronics inside the body and the seeker. In addition, a typical seeker is constructed by a blunt nose which results in an increased wave drag levels. Therefore, using an additional front cover to protect the missile's nose and its clear separation from the missile's body are an important issue mainly for air-to-air and surface-to-air types missiles.

Accurate predictions of missile's canopy separation trajectory is very important for the canopy's design since an unsuccessful separation may damage the missile and lead to a catastrophic failure. An air-to air missile operates in various angle of attack, side slip angles and high Mach numbers. Ejecting the missile's canopy in these hostile conditions could endanger the missile. Originally, these trajectory predictions are obtained by using wind tunnel experiments. However, since high cost and complexity are involved in this approach, it leads missile researchers to find faster and reliable methods. For this aim, and because of the increasing computer technology, researchers have been concentrated on numerical methods of multi-body dynamic simulations were the motivation of this paper comes from.

Rigid body and flow dynamics problem have already been handled by Wang and Kannan [1] and recently by Shau et. al [2]. The later developed a method for complete aerodynamic canopy's ejection by using time accurate simulations. Time accurate CFD has been performed to compute the unsteady aerodynamics of spinning projectiles, coupled with rigid body dynamic to compute the projectile free flight at supersonic speeds.

The body dynamics and fluid mechanics coupling is a very challenging task for the time accurate simulation. Dash and Cavallo [3] studied experimentally and computationally the dynamic of canopy's separation at supersonic flight conditions, and they reported a very good agreements between experiments and CFD calculations, mainly in the initial stage, where the canopy is very close to the missile body. They used overset chimera methods with unstructured mesh approach for simulating the canopy's movement. In this way they could use the advantage of adaptive mesh refinement during the separation process. Whalley [4] developed a canopy that its two halves are affected perpendicular to the flight path in order to increase the STAR II launch vehicle capability. The canopy's surface was coated with an ablative shield to withstand high temperatures. The separation system development included full scale separation tests. Valuable tests results were incorporated into the flight shroud and flown successfully.

Panetta et. Al [5] designed devices to remove the canopy halves at the end-game activities by applying forces that causes the canopy to eject away from the missile. They demonstrated pyrotechnic and hydraulic methods that can be implemented depending on the canopy-missile physical constraints. A protective shroud for an endoatmospheric ground – based interceptor has been designed and tested by Sumb [6]. The separation process shown to consist of fill, venting and high pressure periods. Steady and unsteady aerodynamic time scaling parameters calculated, and good comparisons to experiments are presented.

Recently, Dagan and Arad [7] handled the problem of coupled rigid-body and flow dynamics. The configuration of the ejected shroud was designed using a novel approach, which included only a small amount of wind-tunnel experiments, coupled with aerodynamic model produced by computational fluid dynamics. A simulation of flow dynamics, coupled with rigid-body motion, was developed and tested. They also produced a large aerodynamic database using quasi-steady computations, for hinged and free flight canopy at supersonic flight conditions. This database was used by a six-degree-of-freedom simulation for predicting the canopy's trajectories in various flow conditions.

The aim of this paper is to present an infrastructure construction for canopy-missile separation simulation, in order to accurately predict the safe separation of canopy from a generic missile under various flow conditions: various angles of attack, high dynamic pressure (low altitudes), side-slip angles and high Mach number. This is accomplished by two approaches. The first includes a large quasi-steady CFD database for aerodynamic forces and moments which is coupled to a 3DOF rigid body simulations in order to predict the canopy's trajectories. The second approach includes a multi-body dynamic (6DOF) CFD simulation of the canopy's movement in various flow conditions. The two approaches are compared and evaluated. It is important to emphasize here that the solution approach we took here is more interesting than the specific application. Instead of highly complex aerodynamic CFD simulations, we undertook a simple quasi-steady assumption. The aerodynamic damping coefficient is unknown and we made an assumption that it's behavior is related to the angle of attack value. Then we calibrated this model using the complicated CFD runs, and made comparisons to our approach and realized that results compared well.

Conventional canopy ejection systems typically rely on pyrotechnic devices to release the canopy halves. The canopy is configured to remain coupled to the missile during most of the flight, and to separate at the end-game phase. The canopy hinges are designed to break at specific opening angle.

## II. PROBLEM FORMULATION

The purpose of this paper is to construct a coupled CFD-3DOF simulation tool to investigate the safe missile-canopy separation process in a given flow conditions. The simulation process is composed of two separated unconditioned phases which are finally complement each other:

1. A Monte-Carlo 3Dof simulation code in order to calculate the rotational and translational displacements of the body. Forces and moments which are acting on the body are used in the general equations of motion. This 3DOF code is coupled to an aerodynamic model that incorporates the aerodynamic coefficients of the moving body during its trajectory. For this purpose a large aerodynamic data base is constructed in various angles of attack, side sleep angles, and canopy-missile relative locations. The main advantage of this approach is that the at the moment you have an aerodynamic detailed model, a large 3Dof Monte-Carlo simulations can be performed with much lower computational cost compared to a detailed CFD analysis. The canopy-missile separation process includes three stages:
  - A. **Hinged model**- In the first stage the canopy is fixed to the hinge at an opening angle of  $\theta = 20^\circ$  with respect to the symmetry plane (see Figure ). This is the starting condition.
  - B. **Proximity model** - The canopy separation starts in a very fast movement mainly in the Z direction. In this stage the canopy flow field is computed in different locations (x and z directions) with regard to the missile's body.
  - C. **Free-body model** - The third stage actually starts when the canopy center of mass is located 2-3R away from the missile where R is the missile's radius. In this stage the aerodynamic coefficients are evaluated in different side-slip angles and angles of attack.
2. In the second phase an unsteady and dynamic (6DOF) CFD simulation of the canopy's movement in various flow conditions is performed. In order to solve the multi-body dynamic problem the commercial software Fluent is used. Finally, results of both phases are compared and evaluated.

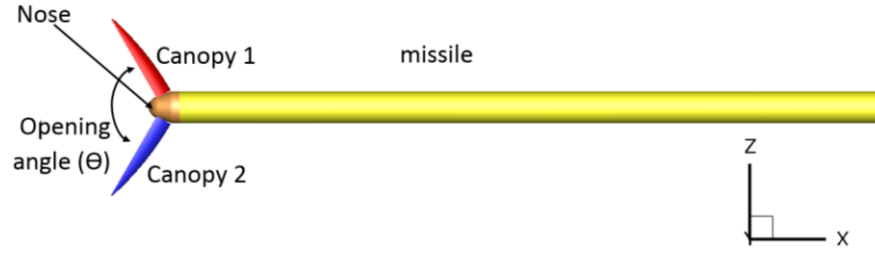


Figure 1: Missile diagram with nose panels

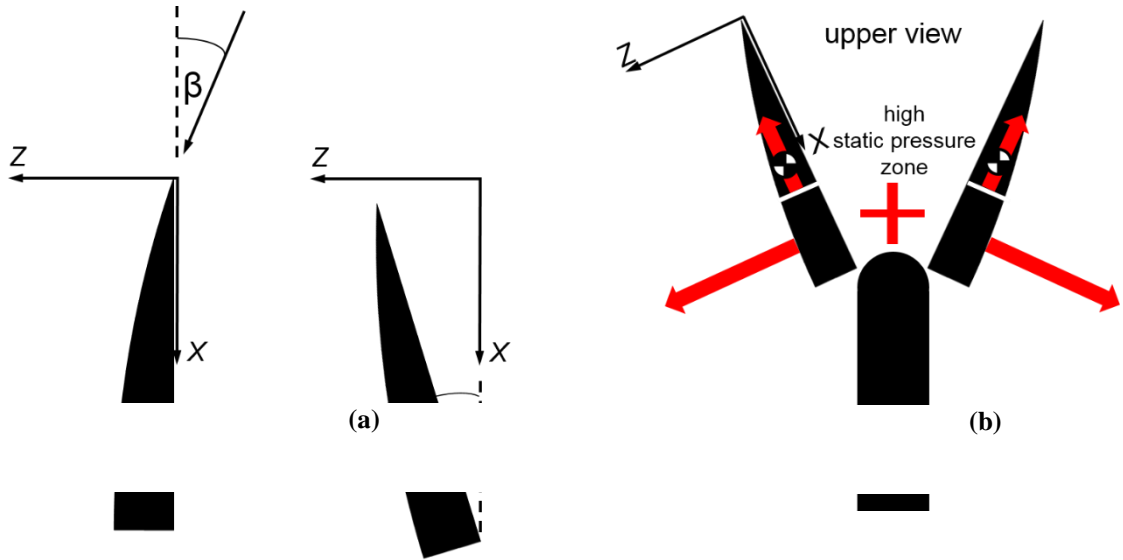


Figure 2: (a) Coordinate system and definition of the opening angle ( $\theta$ ) and side slip angle ( $\beta$ ) (b) A top view of the missile-canopy and the high pressure obtained before separation

### III. COMPUTATIONAL MODEL DESCRIPTION

#### A. Geometry

The computational model consists of three main components: hinged canopy, missile nose and missile body, as is shown in Figure . The canopy has ogive-type cross-section at the front body and flat type cross section at the aft body. The canopy is rotated in a  $\theta = 20^\circ$  with respect to the x-axis in x-z plane. This configuration is the initial position for all the simulations. The missile fins eliminated from the computational model, and the coordinate system is located at the tip of the closed canopy (if it was rotated at  $\theta = 20^\circ$  backward around y-axis, see Figure ). The far-field is located  $25D$ , where  $D$  the missile's body diameter.

The first stage, where the canopy is hinged, a full configuration is used in order to evaluate the effects of side slip angle and angle of attack, and also to solve the right effect of the other canopy on the moving one. The second and third stages, were zero side slip angle was involved, a symmetry surface was used.

#### B. Boundary conditions and flow solver

The steady state flow field computations were performed using Sumb flow solver, which is a finite volume, cell-centered multiblock solver for the compressible Euler, laminar Navier-Stokes, and RANS equations (steady and unsteady). Sumb provides options for a variety of turbulence models with one, two and four equations and options for adaptive wall functions. Sumb has been used extensively for subsonic, transonic, supersonic and hypersonic flow configurations. The discretization of the governing equations is done by a finite volume approach with a central formulation over structured meshes. The convective terms are computed by Roe flux splitting upwind scheme with Van-Albeda limiter. Viscous fluxes

are computed to second order accuracy using a central difference approach. The residual smoothing is made by employing an explicit 5th order Runge-Kutta algorithm. The computational coordinates are  $x$ ,  $y$  and  $z$  axes, while  $x$  is in the stream-wise direction,  $y$  vertical, and  $z$  span-wise. The origin is located at the canopy tip stagnation point (in a closed position, see Figure ). In order to accelerate convergence, a geometric multigrid and residual averaging were used. The turbulence model and the viscous fluxes are calculated on the finest mesh level and consequently transferred to the coarse grid. The solution was done in parallel using Message Passing Interface (MPI) library on a cluster of X86 processors.

The boundary conditions are represented in Figure . All side-boundaries except the right side were set as far-field, with a standard atmosphere model for sea level altitude, temperature and pressure free stream conditions. The first and third stages (hinged canopy and free-body models) were simulated by a full configuration, therefore the right-side boundary was set as far-field, while the second stage (proximity model) was simulated with half configuration and the right-side boundary was defined as symmetry plane. The canopy, nose and missile's body were modeled as solid wall boundary with non-slip velocity.

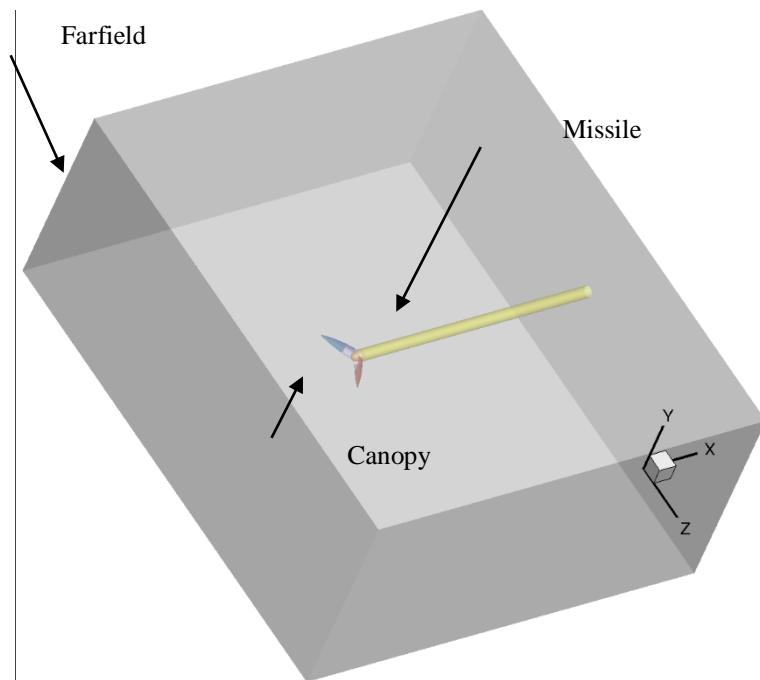


**Figure 3: Dimensions and coordinate system of the computational model**

### C. Computational Mesh

Since the simulation process is decomposed to three stages that differ one from the other in the missile-body orientation, three different grid topologies were conducted in order to get an appropriate grid for the specific stage. The rotated canopy with respect to the missile's axis and the canopy's complicated geometry, gives rise to complicated flow features. Since the canopy's movement is mainly effected by the pressure forces (which can be classified as an Eulerian mechanism) and not dissipation forces, the influence of the mesh clustering near the wall boundaries is modest and has negligible effect on the forces developed on the canopy. The dissipation forces become dominant while the canopy's angle of attack is increased which leads to flow perturbation and boundary flow separation. In this case the drag generated by the canopy is increased and the trajectory may well be effected. For this reason it is extremely important to use a sufficiently refined computational mesh, where the boundary layer is well captured.

Both the first and third stages characterized by full configuration structured grids. For each configuration the same grid is used while the side slip angle and the angle of attack were varied by an appropriate velocity vector definition. The second stage, the proximity model, where the canopy location is varied in a different stream-wise ( $x$ -direction) and lateral (coordinate  $z$ ) directions, is solved by overset mesh approach. In this way five lateral canopy locations (relative to the missile) were analyzed. Nearly 25 cells are created to resolve boundary layer flow, and first point of the surface is chosen

to give  $y^+$  value of about 10. In the volume the mesh growth rate is preserved below 1.16. The second stage is computed by an overset mesh approach. An example of the computational grids for the first stage is presented in Figure .

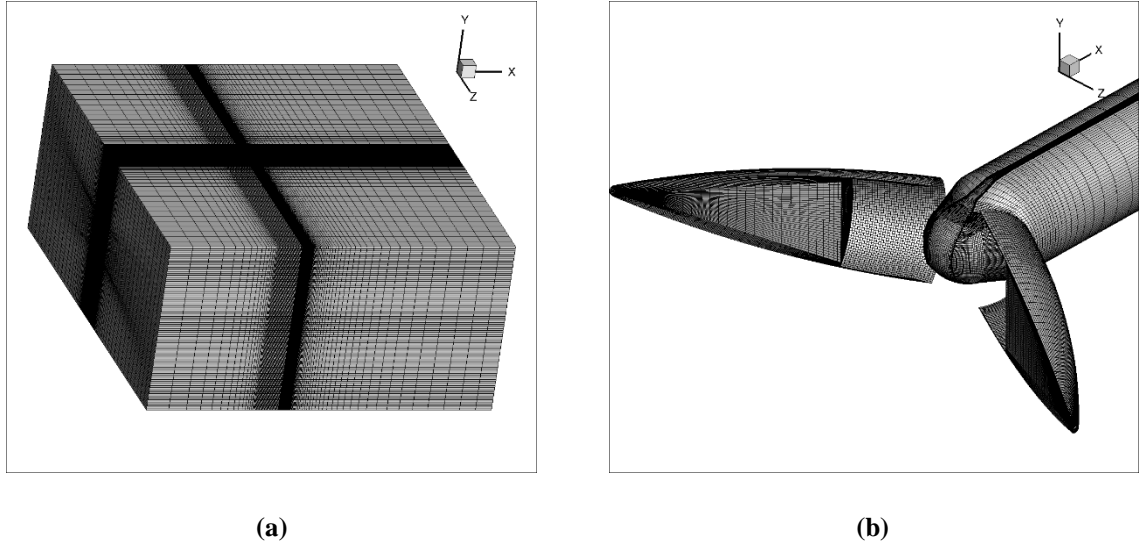


**Figure 4: Volume grid of the farfield (a) and surface grid on the canopy and missile (b)**

Grid convergence study has been made for the three stages, based on the Grid Convergence Index (GCI) method, for examining the spatial convergence of CFD simulations presented in the book by Roache [8]. Roache suggests a GCI to provide a consistent manner in reporting the results of grid convergence studies and also an error band on the grid convergence of the solution. This approach is also based upon a grid refinement estimator derived from the theory of Richardson Extrapolation [9]. The GCI on the fine grid is defined as:  $GCI_{fine} = \frac{F_s}{r^p - 1}$  where  $F_s$  is a factor of safety (recommended to be  $F_s = 1.25$  for comparisons over three or more grids). The GCI for coarser grid is defined as:  $GCI_{coarse} = \frac{F_s r^p}{r^p - 1}$ , while each grid level yield solutions that are in the asymptotic range of convergence for the computed solution. The parameter  $p$  is the order of convergence (here a second order accuracy is involved, so theoretically the maximum value is  $p=2$ ), and  $r$  is the effective grid ratio:  $r = \left(\frac{N_1}{N_2}\right)^{1/3}$  where  $N$  is the total number of grid points in executive grid levels. The asymptotic range of convergence can be checked by observing the two GCI values as computed over three grids,  $GCI_{23} = r^p GCI_{12}$ , while values approximately unity indicates that the solutions are within the asymptotic range of convergence.

For this purpose several levels of grid refinement have been checked to assess the effect on the numerical accuracy, while the total grid cells number:  $N_2=200704$ ,  $N_1=438656$  and  $N_0=1044480$  cells. The grids generated with clustering cells near the walls which results in a maximum of  $y^+=1$  in all the computed angles of attack. The grid convergence study was conducted on the free-body canopy as well as the hinged model (first stage).

A polar graph of the normal force and the pitch moment coefficients are presented in Figure ,Figure . The GCI values including the asymptotic range of convergence and an estimation of the aerodynamic coefficient values at zero grid spacing are detailed in Table 1, computed at the demanding flow condition of  $\alpha = 15^\circ$ . Based on this study we can say, for example, that  $C_y$  is estimated to be  $C_y = 0.3548$  with an error band of 0.0514%. The grid resolution studies confirmed that the computed aerodynamic coefficients values are grid converged.

**Table 1: Aerodynamic coefficient evaluations for Grid convergence study computed in  $\alpha = 15^\circ$ .**

Grid level	Grid ratio, r	GCI [%]	Richardson extrapolation	Asymptotic convergence
N0	1	-		

$C_m$	N1	1.297	0.003659	-0.4728	1.384
	N2	1.732	0.040820		
	N0	1	-		
$C_y$	N1	1.297	0.051476	0.3548	1.220
	N2	1.732	0.160433		
	N0	1	-		
$C_x$	N1	1.297	2.408	0.2036	1.149
	N2	1.732	3.116		

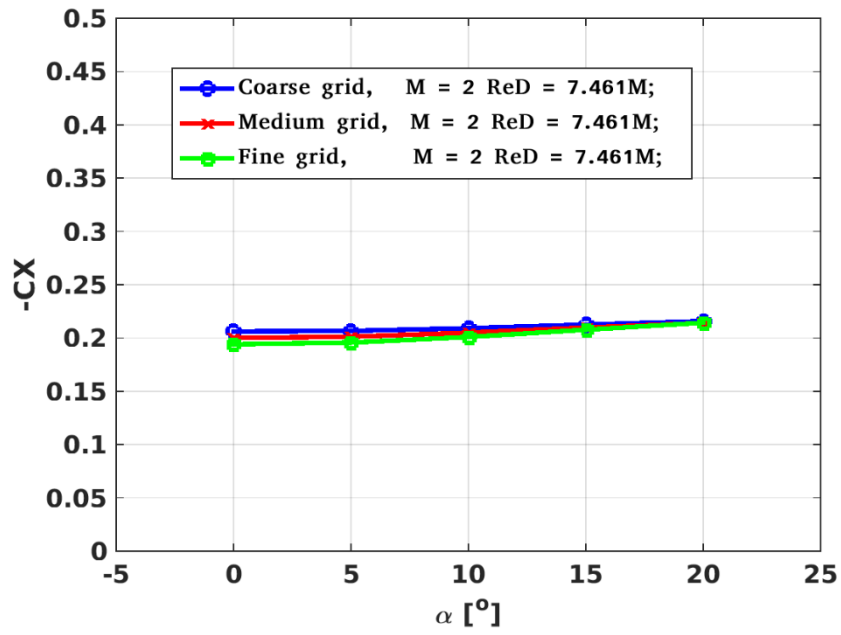
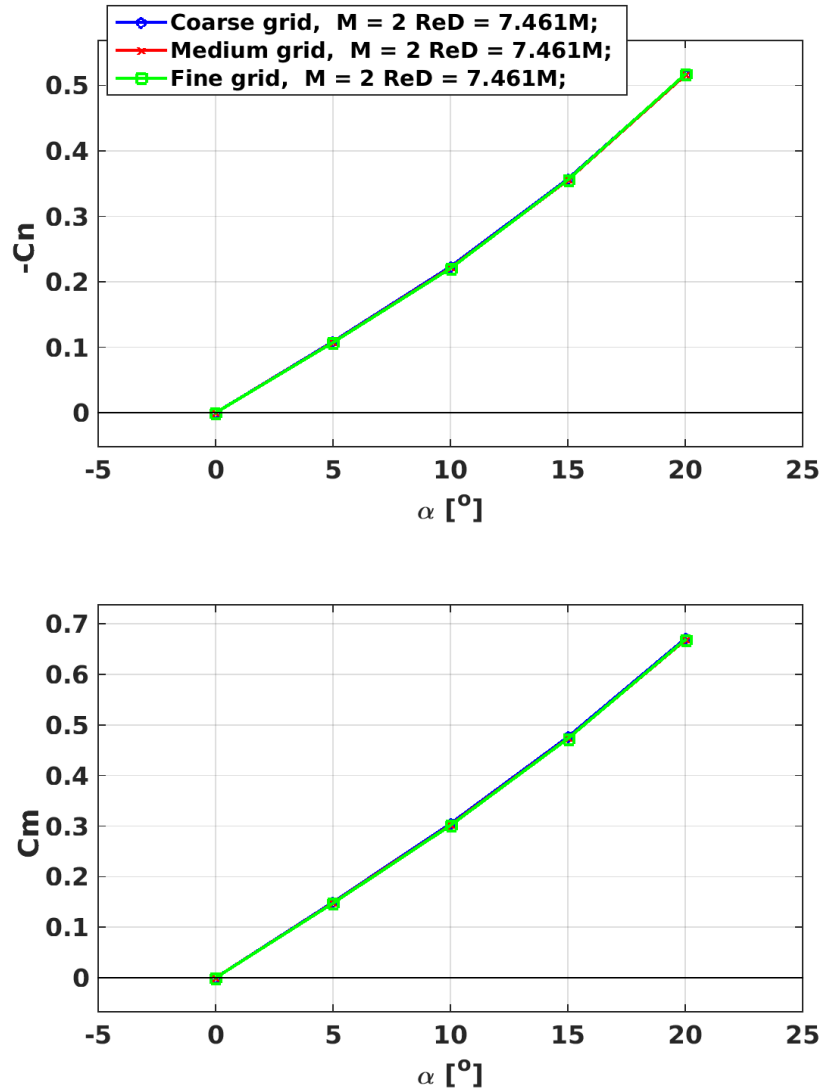


Figure 5: Axial force coefficient with respect to the angle of attack for free-body canopy computation (third stage)



**Figure 6: Normal force and pitch moment coefficients with respect to the angle of attack for free-body canopy computation (third stage)**

#### **D. Aerodynamic coefficients data base generated for the aerodynamic model**

The data base for the canopy's separation process was generated for a steady, compressible and turbulent flow using Sumb flow solver with structured body fitted grid methodology. The CFD analysis are performed in  $M = 2$  at sea level for the three stages. The detailed flow conditions are presented in Table 2. A total of 35 simulations were conducted for various angles of attack, side sleep angles and canopy-missile relative locations, and the simulated configurations are detailed in Table 2. At the first stage, canopy's-hinged model, before the canopy is released a very high pressure values are obtained at the area between the canopy and missile's front, and it is clearly seen in

Figure . These pressure gradients are mainly a result of complex shockwaves interactions on the canopy and the missile's nose. A hinged-model steady state pressure coefficient is presented in Figure (a) for both  $\theta = 20^\circ$  and  $\theta = 40^\circ$  canopy's location. At the bottom figures the free-body model is presented for comparison. It is clearly seen that the numerical solution of the flow fields is highly sensitive to the grid refinement, the ability to predict f the local normal shock, and the correct shock layer are the most critical aspects of the present simulations.

**Table 2: A list of the simulated configurations**

Configuration	Angle of attack (deg)	Side slip angle (deg)	Opening angle (deg)	Canopy's dz location
Missile body+canopy	-15:15	0, 1, 5	2.5, 5, 10, 15, 20, 40, 60	-
Proximity model	0, 5, 10	20	-	3R, 4R, 6R, 10R
Canopy as a free body	-50:5:50	-75:10:75	-	-

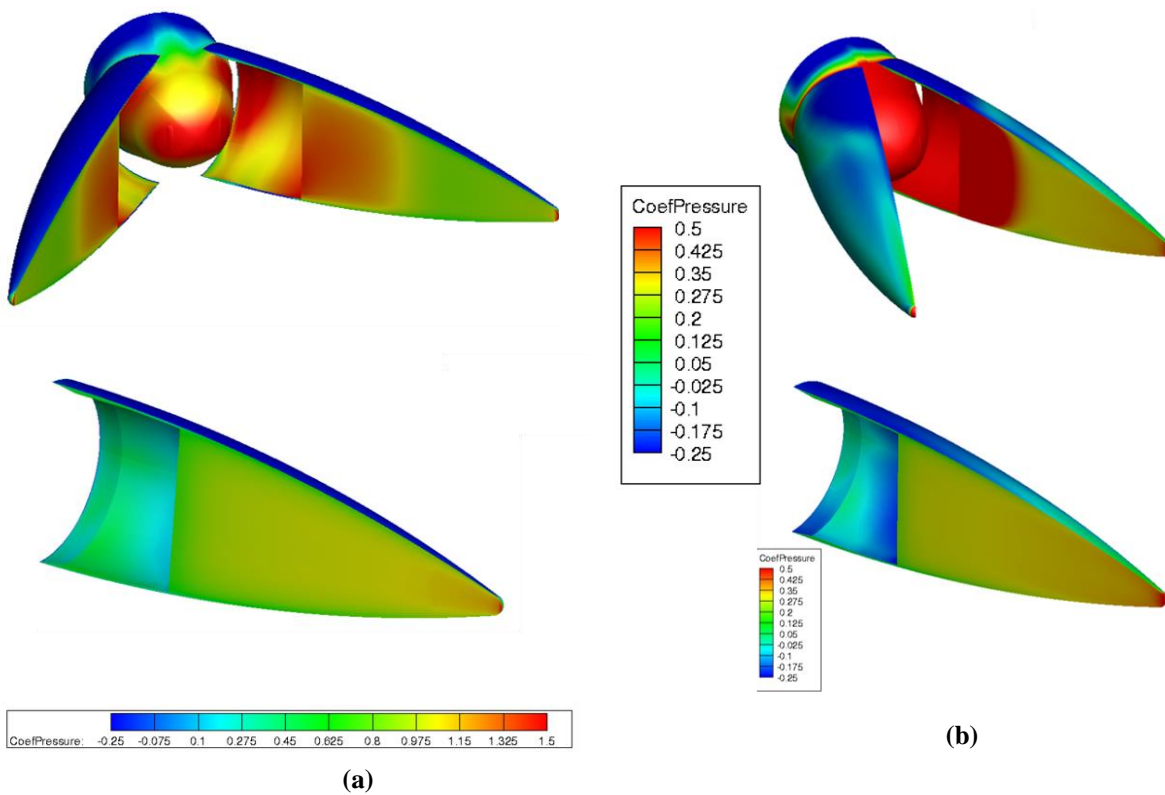


**Figure 7: Pressure coefficient values computed at  $\theta = 40^\circ$  (a) and  $\theta = 20^\circ$  (b). The top figures represents the proximity model and bottom figures represents the free-body model.**

**Table 3: Canopy's physical characteristics and flow conditions**

Free stream Mach number	2.0
Missile angle of attack, [deg]	0, 10
Static pressure, [Pa]	101325.0
Initial radial velocity, $w_{0y}$ , [rad/s]	100
Initial linear velocity, $V_{0z}$ , [m/s]	15

## IV. 6-DOF MODELING AND MONTE-CARLO SIMULATIONS

The 3Dof model is constructed based on the following assumptions:

1. The canopy's trajectory is planar and as a result three degrees of freedom are involved: the X and Z force coefficients ( $Cfx, Cfz$ ) and the moment in Y direction ( $Cmy$ ).
2. The canopy aerodynamic characteristics are obtained by quasi-steady CFD analysis.

The canopy trajectory calculation is based on numerical integration of 3DOF equations of motion. Two translational axes (longitudinal and lateral) and one angular dynamic equation. The main assumption is that the canopy's motion out of plane, during the initial phase of the motion, is negligible.

The equations of motions are the conventional 3DOF differential equations for a rigid body with constant mass and moments of inertia were solved in order to obtain the linear and angular velocities, including the body's displacements in a delta time step size. The equations of motion are  $\vec{F} = m \frac{\partial \vec{v}}{\partial t}$ ,  $\vec{M} = m \frac{\partial \vec{h}}{\partial t} + \omega \times \vec{h}$ , where  $m$  is the body mass,  $\vec{v}$  is center of gravity linear velocity,  $\vec{h}$  is angular momentum,  $\vec{\omega}$  is angular velocity about the body's center of gravity. The key aspect of the canopy dynamics is a proper modelling of the aerodynamic forces and moments acting on the canopy. The fact that the canopy is characterized by low inertia (mass and moments of inertia) emphasizes the need for proper aerodynamic model, since high translation and angular accelerations are involved.

The aerodynamic model is based on flow simulations (RANS) that were undertaken for a free-body canopy and a canopy that is in the near vicinity of the afterbody. The flow simulations show that most of the region of influence of the afterbody is when the canopy is less than one reference radius from the afterbody. Thereafter, most of the aerodynamic characteristics are of a free-body canopy. The physical explanation for that is the high pressure that is developed at the inner surface of the canopy in the initial stage of the canopy's opening. These high pressure values apply thrust-like phenomenon (instead of typical drag) and an aerodynamic moment that induces the canopy's closing. The later phenomenon highlights the opposite aerodynamic mechanisms during the canopy's motion; the first apply canopy closing while later on the aerodynamic moments changes and promote canopy opening. This also highlights the importance of proper initial conditions after the pyrotechnic opening of the canopy. Lastly, the canopy trajectory is influenced by two additional factors: the aerodynamic damping mechanism, since the increased angular velocities, and the trim angle, which is largely influenced by the location of the center of gravity.

In order to validate the proposed aerodynamic model and to properly choose the decay model coefficients that interpolate the aerodynamic coefficients between the perturbed and unperturbed regions, a full dynamic and flow simulation was undertaken. Once the aerodynamic decay model was formulated, the ODE45 (Matlab based) integration scheme was used to integrate the equations of motion.

### A. Aerodynamic model characteristics

#### 1. Comparison between first stage (free-body motion) and third stage (hinged-model)

The aerodynamic model which is based on the quasi-steady CFD simulation is presented in the following figures. The axial force ( $C_x$ ) with respect to the side slip angle ( $\beta$ ) is presented in Figure for right and left canopy's, calculated at  $\alpha = 0^\circ$  and  $\alpha = 10^\circ$ . These figures expose the complicated flow that acts on the missile-canopy configuration and especially in the first stage where the canopy is still mounted to the hinge. Let us analyze the left free-body canopy. For

$\beta < 30^\circ$  generate a positive axial force which tends to close the angle, for higher side slip angles the axial force is negative due to flow separation which generates high pressure values on the curved side. The hinged-model, on the other hand, exhibits negative axial force coefficient in all the side-slip angles. In addition, for  $\beta > 20^\circ$  the axial force stays nearly constant because of the high pressure values and shock waves created by the missile's nose, which are more dominant than the side-slip flow effects.

The y-moment coefficient ( $C_{m_y}$ ) with respect to the side-slip angle ( $\beta$ ) is presented in Figure for right and left canopy's, calculated at  $\alpha = 0^\circ$  and  $\alpha = 10^\circ$ . For the hinged-model, the mutual influence of the missile nose-canopy is clearly seen with a high moment coefficient values compared to the free-body model. The influence of the angle of attack is neglected. It is interesting to see that the moment coefficient changes sign at  $\beta > 0^\circ$ , unfortunately this feature exists for all the hinged-model aerodynamic coefficients.

The side force coefficient ( $C_z$ ) with respect to the side slip angle ( $\beta$ ) is presented in Figure for right and left canopy's, calculated at  $\alpha = 0^\circ$  and  $\alpha = 10^\circ$ . As expected the additional pressure values obtained in the missile nose-canopy configuration results in higher side force values compared the free-body model. The side slip angle effect is clearly demonstrated in

Figure for  $\beta = 2^\circ$ . From the illustration of the canopy's position we can see that right canopy, in a positive side-slip angle, experiences higher axial force values and therefore drifted further downstream.

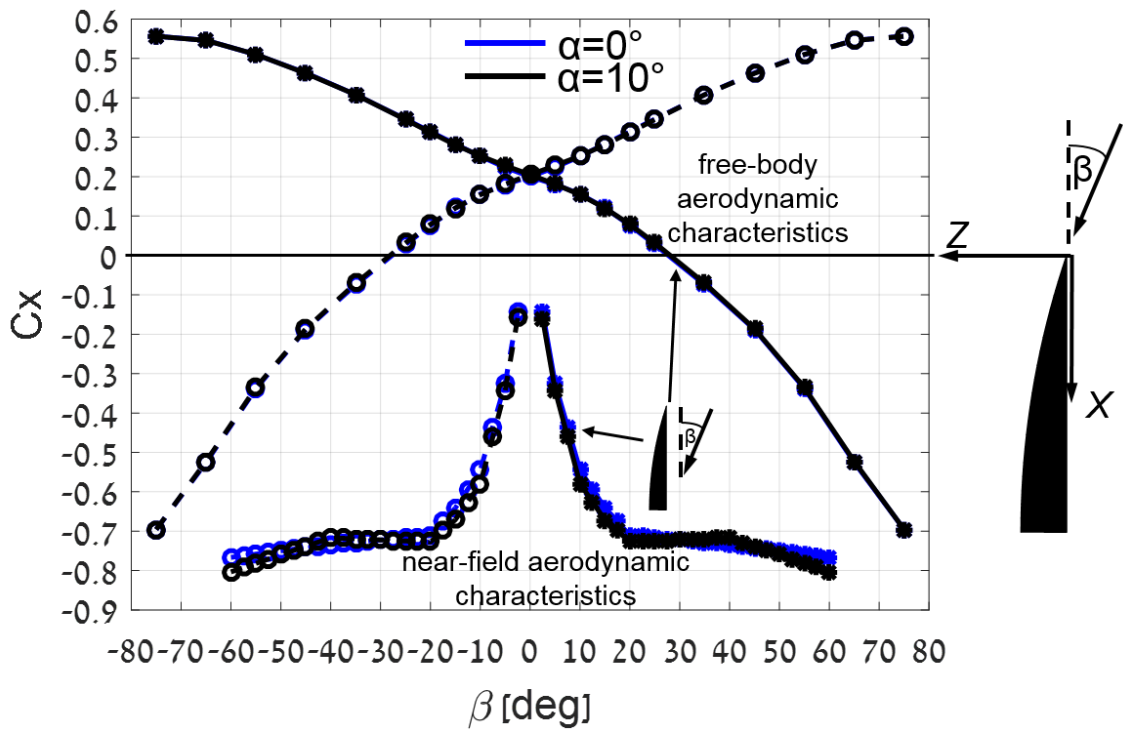


Figure 8: Axial force for free-body and hinged-model, for two angles of attack

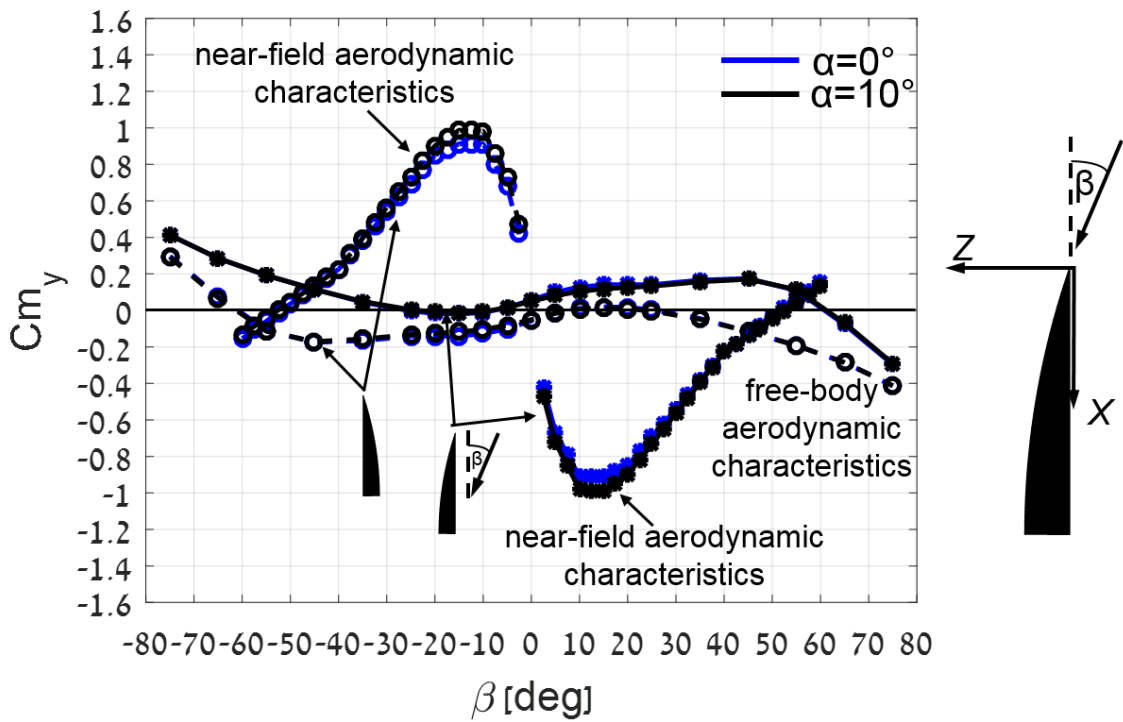


Figure 9: The Y-moment coefficient for free-body and hinged-model, for two angles of attack

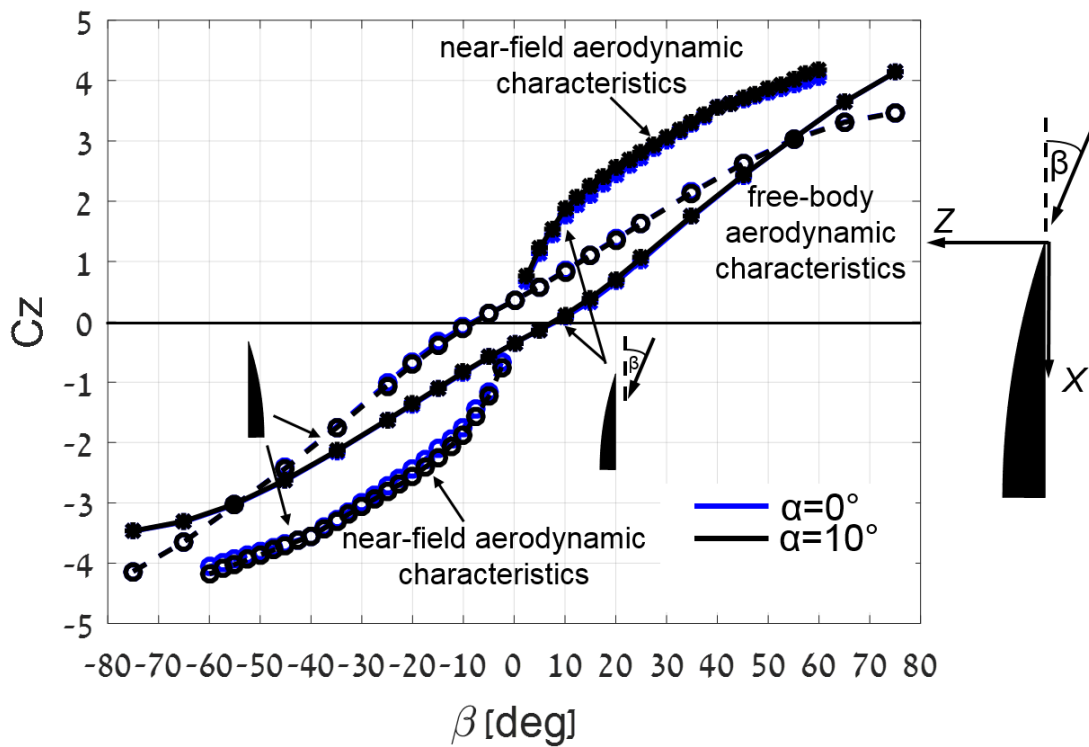


Figure 10: Force coefficient  $C_z$  for free-body and hinged-model, for two angles of attack

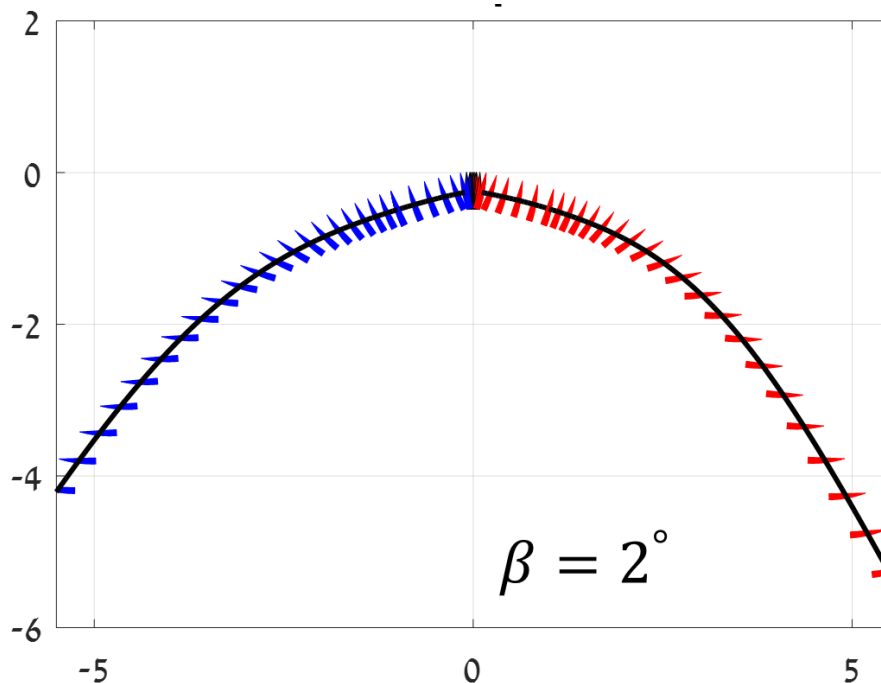
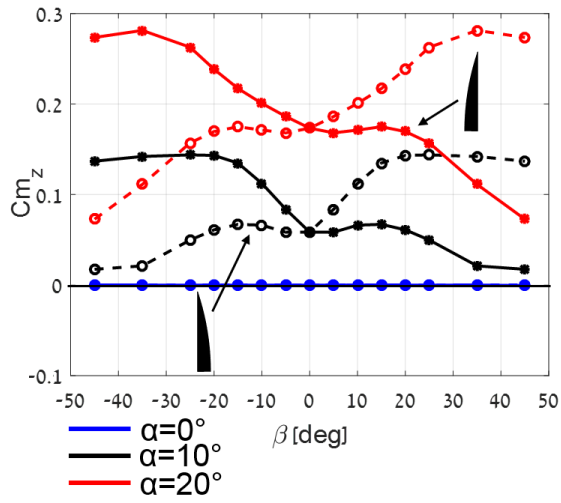


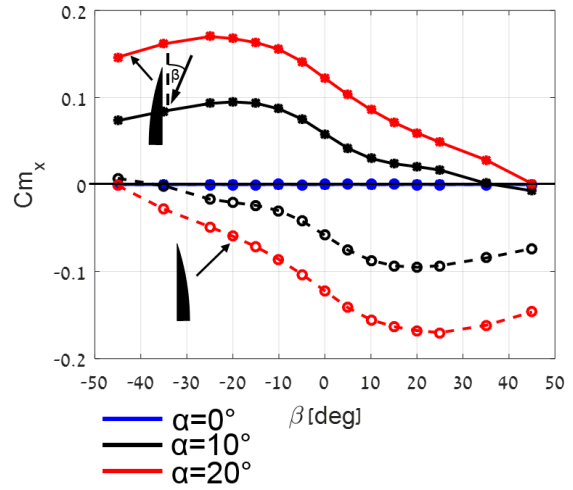
Figure 11: Side slip angle effect on the right and left canopies, simulated at  $\beta = 2^\circ$

## 2. Free-body model characteristics in different angles of attack

The following figures presents the aerodynamic coefficient (forces and moments) of the free-body model for three angles of attack  $\alpha = 0^\circ, 10^\circ, 20^\circ$  with respect to the side slip angle. The main interesting feature in this model is that the  $C_y$  values are nearly order of magnitude lower than the side force coefficient ( $C_z$ ) values. This emphasize the fact that the canopy's movement is mainly planar, and the 3Dof model is a good choice for this flow configuration.

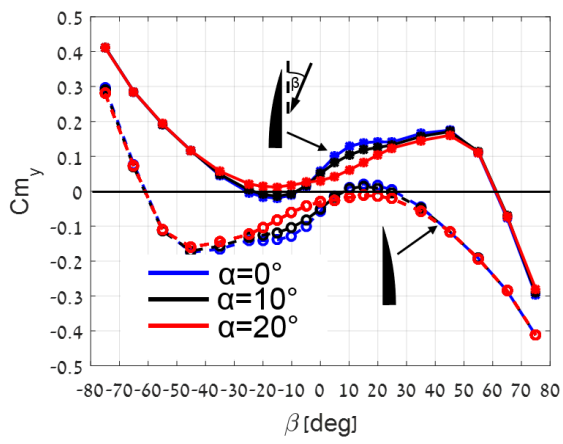


(a)

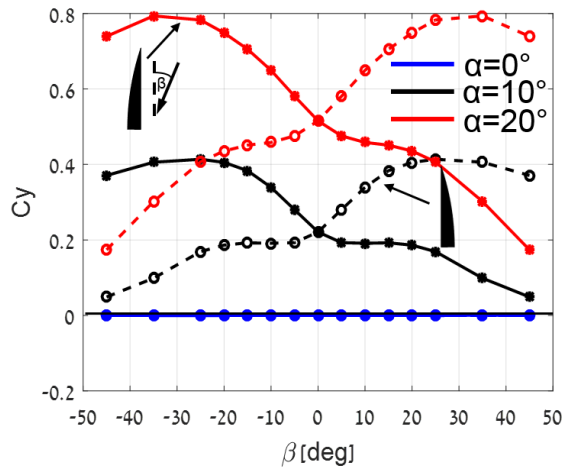


(b)

Figure 12: Moment coefficients Versus side slip angle for three angles of attack



(a)



(b)

Figure 13: The Y-moment coefficient (left) and force coefficient (Right) versus side slip angle

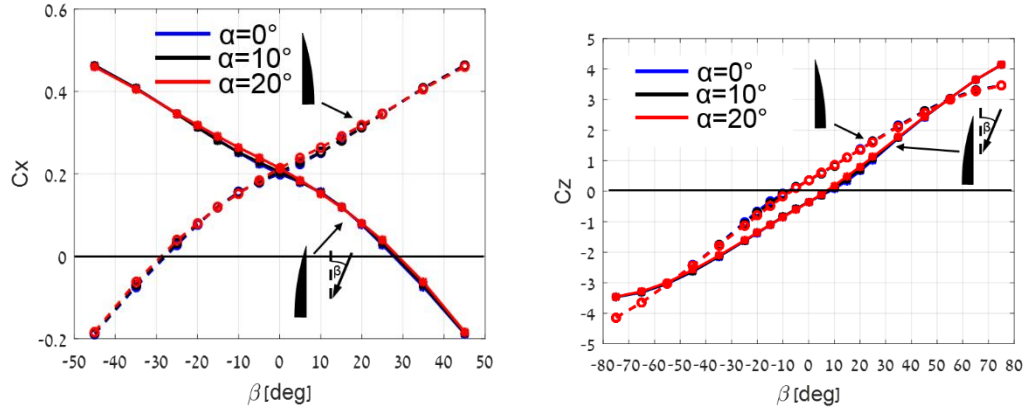


**Figure 14: Axial force coefficient (left) and z-force (right) coefficient versus side slip angle**

## B. Canopy trajectory calculations by a moving mesh approach

### 1. Computational grid generation and flow solver

The related numerical simulation of the canopy's trajectory is performed for the same configuration but with three approaches. The first trajectory obtained by solving the compressible Euler equations. These results were compared to a second solution obtained by solving RANS. Since those simulations obtained with a 0 angle of attack, from a simplifications reasons, we had to check whether the canopy's plenary movement assumption is still valid in high angles of attack. For this purpose a third simulation was conducted with  $\alpha = 10^\circ$ .

Computational grid generation for the 3D trajectory simulation phase is carried out in Centaur commercial software. A dynamic hybrid unstructured tetrahedral mesh approach is accomplished by using three grid sizes (coarse medium and fine) to numerically solving and comparing the results of the three dimensional, inviscid and compressible Euler equations and RANS equations with the first phase (3DOF-CFD aerodynamic based model). The mesh quality was iteratively improved by varying the grading type, ratio and interval count for the edge meshing with the aim of having enough grid cells to describe the canopy's movement and also have low skewness values. The hybrid level includes 10 hexahedral cells while the nearest wall cell is located about 1 mm of the wall. In

Figure a surface meshing of the canopy and missile's body configuration is presented. The computational domain is large enough to minimize flow effects between model and boundaries. The far-field boundaries are located 25D from the center of missile body. Downstream, upstream and all side boundaries except right side (pilot view) were set as pressure far-field, using standard atmosphere model at sea level. Right side boundary was defined as symmetric. Solid surfaces (canopy and missile) were modeled as no-slip (except in Euler case), adiabatic wall boundary condition.

The unstructured dynamic mesh is updated by combining spring smoothing and local re-meshing and adaptation. With the dynamic mesh technique, the mesh elements are deformed due to the motion of the canopy during the release

process. In areas where the mesh deformation is small, spring-based smoothing algorithm is employed, and when the deformation becomes large, the mesh elements cannot be stretched or compressed anymore. In this situation, the adaptation algorithm is employed and new grid elements are generated. The static adaptation is done manually, every 1000 time step iterations, based on the static pressure gradient, inside a sphere with a diameter of 1 m with its center located at the canopy's center of gravity. The canopy moves as a rigid body and the edges between any two mesh nodes are idealized as a network of interconnected springs. The initial mesh size is approximately 1250000 cells and the final adapted mesh contains  $3 \times 10^6$  cells approximately.

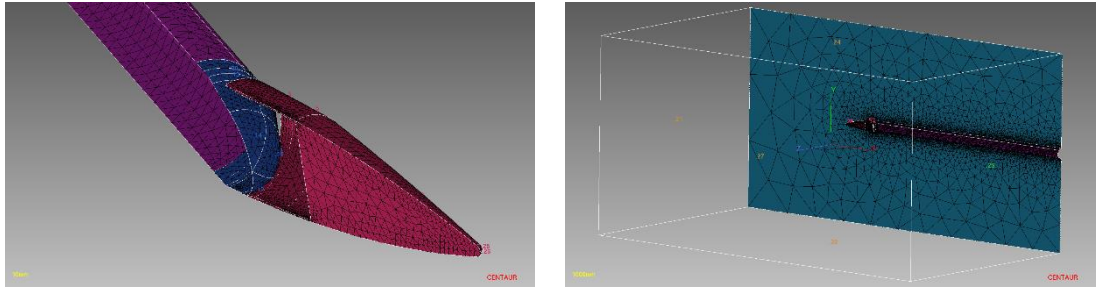


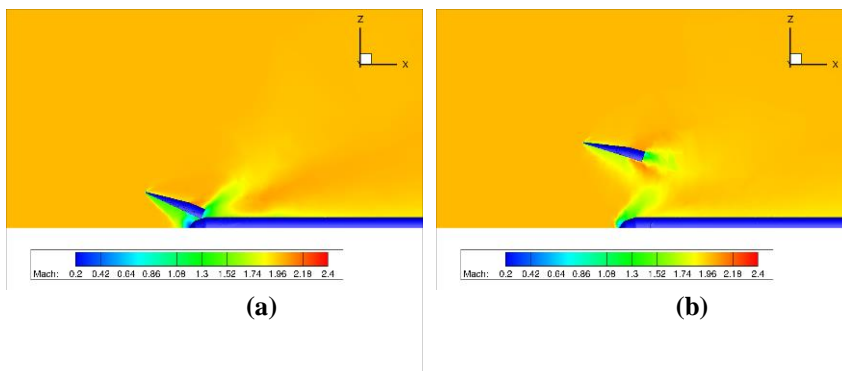
Figure15 : A magnified view of the canopy-body mesh (left), and the volume tetrahedral mesh (right)

### C. Results and discussion

CFD analysis were performed for three canopy-missile configurations at Mach number 2 and at sea level height. The three cases are: inviscid compressible Euler equations at  $\alpha = 0^\circ$ ,  $\alpha = 10^\circ$ , and NS equations with  $\alpha = 0^\circ$ . First, a steady simulation was conducted in order to obtain the correct aerodynamic forces and moments values and compare them with the results of the quasi-steady approach (first phase). Then the solver was coupled with dynamic mesh approach, within Fluent, for the complete canopy trajectory computation. The canopy inertial specification are integrated within Fluent as a user-defined function (UDF). At the starting point the canopy is located in an opening angle (the angle between the canopy main axis and the symmetry plane) of  $\theta = 20^\circ$ . The initial conditions for the simulation, which were verified in experiment, are radial velocity of 106 rad/s (around the hinge) and linear velocity of 15 m/s in the z direction (see

Table 3). It is important to mention here that at these flow conditions, lower initialization values were checked but the developed ejection moment was not enough for the initialization of the separation. The time step defined is  $1e^{-5}$  sec and 20 sub iterations were made for transient analysis. Approximately overall clock time to reach convergence and canopy's separation of nearly 3m in z-direction is about 100 hours, using parallel computer clusters, using 32 CPU's.

Time dependent position and angle orientations are obtained and results are compared with the 3DOF-Monte-Carlo computations (see Figure ). These trajectories reflect position change of the canopy's center of gravity. As it is clearly shown the canopy separation is performed safely for Euler and Navier-Stokes simulations cases. The two cases compares very well mainly in the first 0.003 seconds from release, and both trajectories are approximately the same. As the canopy's angle of attack is increased successive parasite drag is induced because of stall and flow separation, a viscous based phenomena, which are clearly not well captured with the Euler inviscid equations. This is the reason why the canopy's with



the Navier-Stokes equations is drifted backwards, in x direction, more than the trajectory obtained with Euler equations. These results approved that the inviscid flow approximation is sufficient for the trajectory calculations.

**Figure 16: Top views of Mach number contours for canopy separation ( $\alpha = 0^\circ$ ). The simulation time: (a) 2.5ms, (b) 10ms, (c) 20ms**

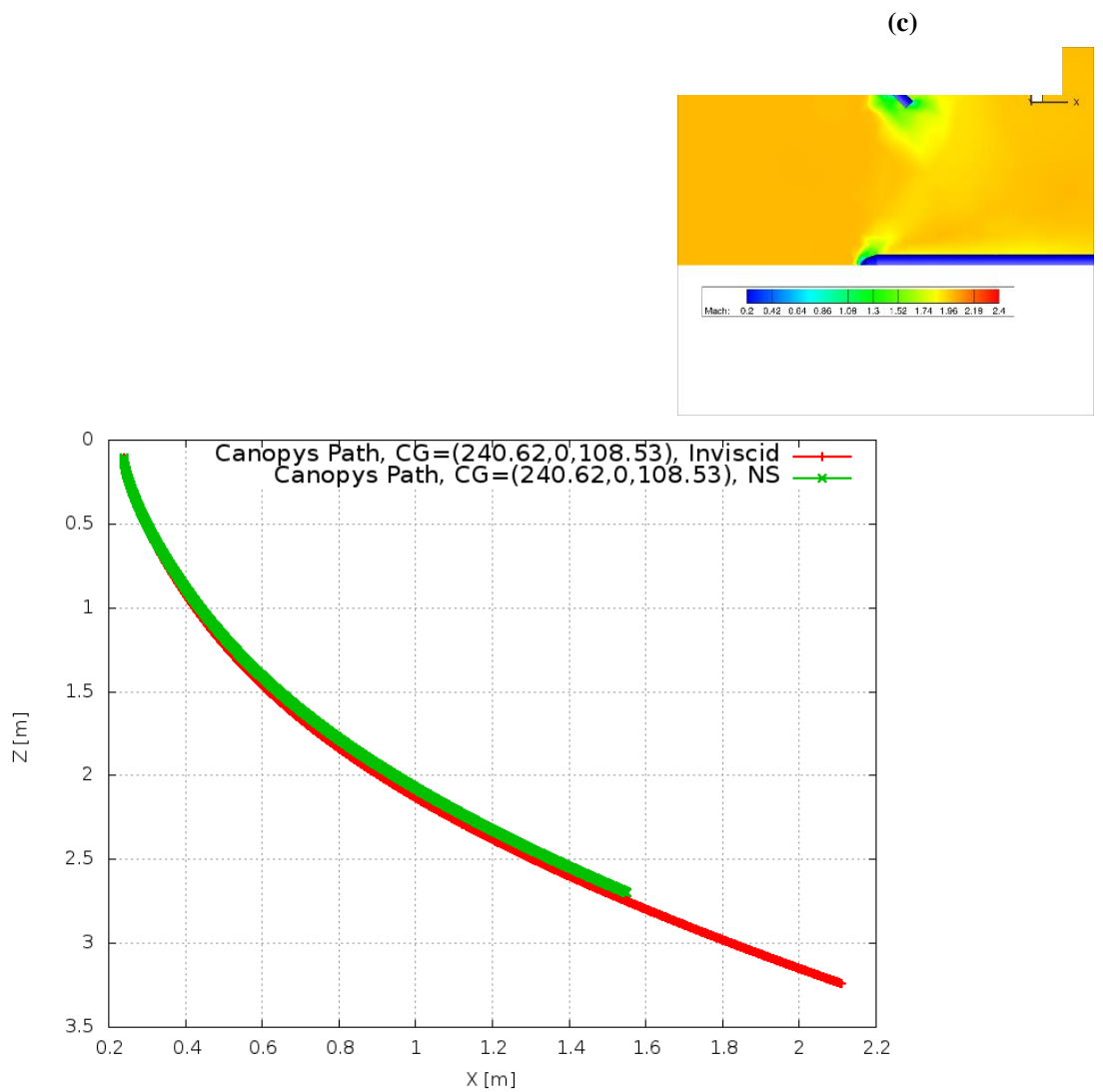


**Figure 17: A comparison between Euler and RANS simulation of the Canopy's trajectory with  $\alpha = 0^\circ$**

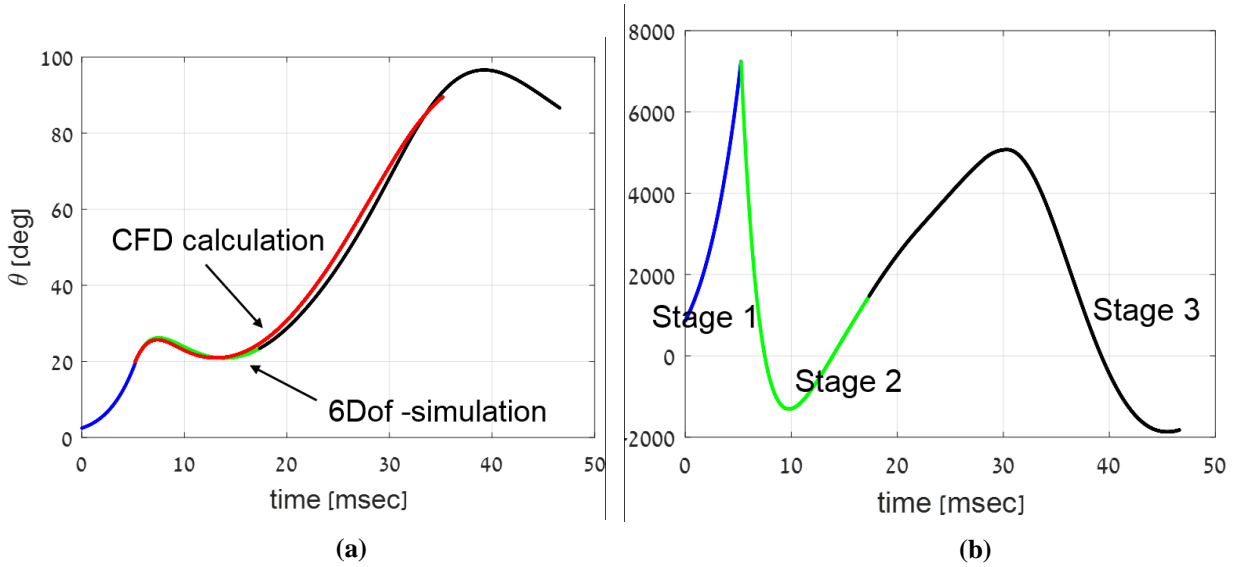


**Figure 18: Comparison between the 3Dof-Monte-Carlo simulation model and unsteady CFD simulation. (a) Opening angle  $\theta$  with respect to time. (b) Opening angle  $\theta$  derivative Vs. simulation time.**

## 2. Trajectory results at $\alpha = 10^\circ$

The main 3DOF-Monte-Carlo model assumption is that at the second stage, when the canopy is released from the hinge and can move freely in space, its movement stays approximately in the same x-z plane. This assumption is well obtained in the first simulation, while the canopy release is in  $\alpha = 0^\circ$ . However, in order to verify this assumption, another simulation was conducted, with  $\alpha = 10^\circ$ . Both simulations results are presented in Figure .

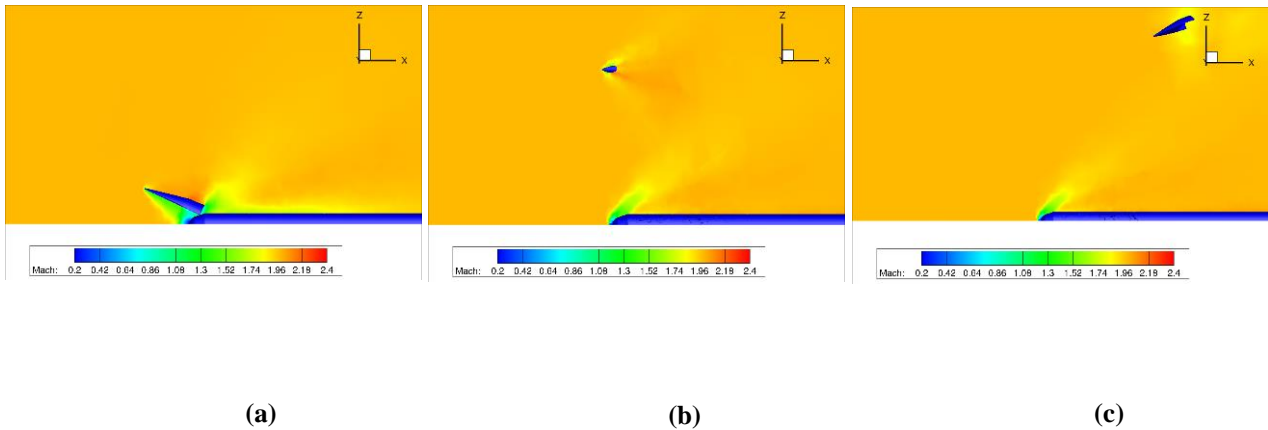


**Figure 19: Top views of the Mach number contours for canopy separation ( $\alpha = 10^\circ$ ). The simulation time: (a) 2.5ms, (b) 20ms, (c) 37.5ms**

(b)

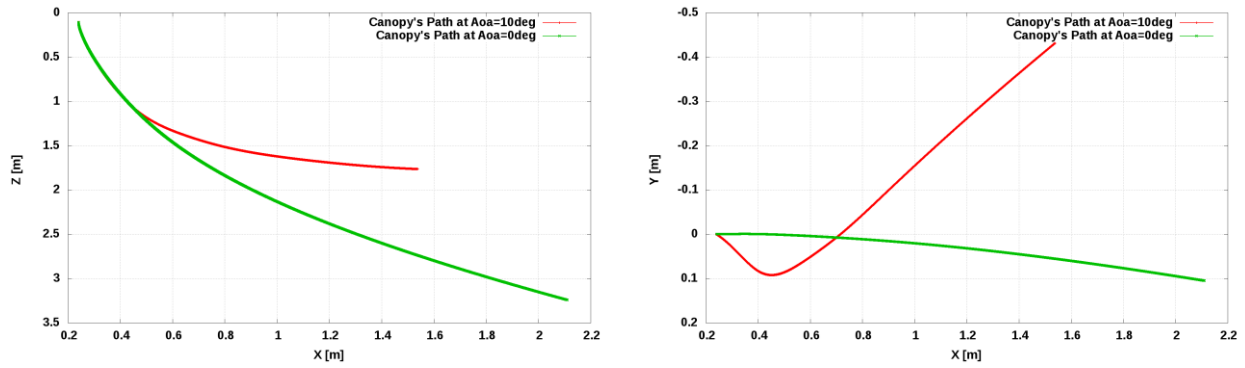


**Figure 20: Canopy's trajectory with  $\alpha = 0^\circ$  and  $\alpha = 10^\circ$  in x-z (left) and x-y (right) planes**

## V. CONCLUSIONS

A computational infrastructure of canopy-missile separation was constructed in order to investigate the safe separation in various angles of attack, side sleep angles and high Mach number. A large quasi-steady CFD database of aerodynamic forces and moments was produced for aerodynamic model formulation, which is coupled to a 3DOF code that incorporates the aerodynamic coefficients of the moving body during its trajectory. The main advantage of this approach is that at the moment you have an aerodynamic detailed model, a large 3DOF Monte-Carlo simulations can be performed with much lower computational cost compared to a detailed dynamic CFD analysis. The solution approach we took here is more interesting than the specific application. Instead of highly complex aerodynamic CFD simulations, we undertook a simple quasi-steady assumption. The aerodynamic damping coefficient is unknown and we made an assumption that its behavior is related to the angle of attack value. Then we calibrated this model using the complicated CFD runs, and made comparisons to our approach and realized that results compared well.

The canopy-missile separation process includes three stages: hinged model, proximity model and free body flow. In addition an unsteady and multi-body dynamic (6DOF) CFD simulation of the canopy's movement in various flow conditions is performed. Results of both phases are compared and evaluated. Although the simulations include a very demanding conditions, under various flow assumptions, the calculated trajectories were in a very good agreement with the 3DOF model. Such a computational infrastructure of this kind is a valuable tool since experiments in these hostile conditions are complex and very expensive. This analysis forms the basis for ensuring the canopy's safe separation and creates a lot of confidence to designers to go ahead for further flight trials at different flow conditions.

## VI. REFERENCES

- [1] Z. J. Wang and R. Kannan, "An Overset Adaptive Cartesian/Prism Grid Method for Moving Boundary Flow Problems," *AIAA*, p. 322, 2005.
- [2] J. Sahu, S. Sifton, D. J. H. K. R. and M. Costelloy, "Generation of Aerodynamic Coefficients Using Time-Accurate CFD and Virtual FLY-Out Simulations," in *DoD HPCMP Users Group*, 2008.

- [3] P. A. Dash and C. S. M, "Aerodynamics of Multi-Body Separation Using Adaptive Unstructured Grids," in *AIAA 18th Applied Aerodynamics Conference*, Denver, 2000.
- [4] I. Whalley, "Development of the STARS II Shroud Separation System," in *37th AIAA/ASME/SAE/ASEE Joint Propulsion Conference*, Utah, 2001.
- [5] A. D. Panetta, "Drag of Shroud Deployment Bladder at Mach Numbers of 8 to 20," *AIAA*, 1999.
- [6] S. B. Lumb, "Transient Aerodynamics of a High Dynamic Pressure Shroud Separation for a Ground-Based Interceptor Missile," in *AIAA*, Alabama, 1992.
- [7] E. Arad and D. Y, "Analysis of Shroud Release Applied for High-Velocity Missiles," *JOURNAL OF SPACECRAFT AND ROCKETS*, 2014.
- [8] P. J. Roache, K. Ghia and F. White, "Editorial Policy Statement on the Control of Numerical accuracy," *ASME Journal of Fluids Engineering*, p. 2, 1986.
- [9] D. A. Anderson, J. C. Tannehill and R. H. Pletcher, *Computational Fluid Mechanics and Heat Transfer*, New York: McGraw-Hill Book Company, 1984.